Experimental and Computational Analysis on Aerodynamic Behavior of a Car Model with Vortex Generators at Different Yaw Angles

G. Shankar[†] and G. Devaradjane

Department of Automobile Engineering Madras Institute of Technology Campus, Anna University, Chromepet, Chennai, Tamilnadu, India.

†*Corresponding Author Email: shankarg1990@gmail.com*

ABSTRACT

Investigating the effects of aerodynamic characteristics in the automotive segment has been one of the thrust areas of research in the recent years. Extensive research had been carried out earlier in minimizing the aerodynamic drag of the car body and to study the effects using passive air flow deflectors. Little work has been conducted on semi-active or actively controlled air flow modification techniques. In order to contribute new knowledge in the chosen area and to draw the attention of current researchers the present work focuses on the study of aerodynamic characteristics of a typical sedan car model equipped with three numbers of delta shaped vortex generators (VGs) as an aerodynamic add-on device to delay the early flow separation of air from the vehicle body. The yaw angles of the VGs are semi actively controlled using mini stepper motors. The middle VG is kept stationary, whereas the other two VGs orientation has been modified and the results have been studied. The aerodynamic property of a car model mounted with four distinct yaw angle configurations obtained by means of mini stepper motor has been quantitatively evaluated by sub-sonic wind tunnel tests and computational analysis. From the experiments the peak drag and lift coefficient reduction rates of 4.53% and 2.55% respectively have been observed in the case of car model with vortex generators having leading edges facing the rear end and the mid plane of the car respectively when compared with the car model without vortex generators. Numerical simulation using realizable (k- ε) model predicted the drag and lift coefficient reduction rates closer to the experimental values and also it predicted the existence of magnitude of turbulent kinetic energy variation in the roof portion of the car model with four dissimilar configurations of vortex generators relative to the case of car model without vortex generators.

Keywords: Drag force; Lift force; Vortex generators; Wind tunnel; Ahmed body; Computational simulation; Stepper motor.

NOMENCLATURE

A	projected frontal area in m^2	L	length of car model in m
C_D	coefficient of drag force	ℓ	characteristics length of model in m
C_L	coefficient of lift force	m	meter
C	VG yaw angle configurations	m/s	meter per second
D	VG Design	N	Newton
F_D	aerodynamic drag force in N	s	second
F_L	aerodynamic lift force in N	VG	Vortex Generator
k	turbulent kinetic energy in m^2/s^2	V	wind velocity in m/s

1. INTRODUCTION

The automobile manufacturers are designing the vehicles to obtain superior fuel economy, good safety and stability even at higher vehicle velocities.

All the above can be achieved by developing the model with an appropriate aerodynamic design. In any automotive system, the improvement of vehicle performance can be achieved in two ways either by redesigning the power house of the vehicle,

transmission and its subsystems or by improving the aerodynamic characteristics of the vehicle whereas it plays a predominant role in determining the comfort and stability of the vehicle. Extensive studies had been conducted in the past to reduce the effects of drag and lift forces in the passenger car segment. Aljure et al. (2014). had carried out a comparative computational study on the Ahmed bluff body and ASMO car geometry by applying four different LES models, namely SIGMA, WALE, QR, VMS being used to simulate the flow around the two different models of which the numerical simulation predicted that in case of Ahmed body the SIGMA and VMS models captured the flow better than QR and WALE models, whereas in the case of ASMO geometry QR and VMS models facilitated better flow simulation than SIGMA and WALE models and on consolidating the present overall numerical analysis, the author had found that among the four LES models, the VMS model exhibits good capability of predicting the flow past to the different geometries similar to car models. Aider et al. (2010) conducted the experimental analysis on the modified curve shaped rear end of Ahmed body instead of regular one with trapezoidal shaped vortex generator as an aerodynamic add-on device and their findings showed 14% reduction in drag force for various wind velocities which would result in lesser fuel consumption. Bello-Millan et al. (2016) carried out experimental analysis on Ahmed body with the rear slant of 25° by varying the yaw angle considering the Reynolds number range lying between 3×10^5 and 30×10^5. It has been found that drag coefficient propagates linearly with increase in yaw angle under constant Reynolds number. Birwa et al. (2013). performed the numerical simulation on AUDI A4 sedan car model for four different wind velocities it was observed that the drag coefficient value was decreasing with increase in wind velocity and minimum coefficient of drag force was observed corresponding to the ground clearance of 101.6mm among the different cases. Castro et al. (2013). performed experimental and computational analysis by applying Detached eddy simulation with Spalart-Allmaras turbulence model in the simplified CAD car model and found that the results were well correlated with the experimental analysis showing error percentage of 13.8% which lies under the allowable error range. Gillieron et al. (2013) carried out an experimental study on Ahmed body in wind tunnel with a rear slant angle of 35° by using pulsed jet actuators mounted on the roof of the rear window. A maximum drag reduction of about 20% was observed from the base model with applied excitation frequency of 500 Hz for pulsed jet actuators. Gopal and Senthilkumar (2013). conducted the numerical study on a typical square back car model incorporated with vortex generator on its roof and without vortex generator. The authors had reported that the intensity of wake region behind the vehicle model reduced significantly for the model having VG and resulted in increased vehicle fuel efficiency. Guilmineau (2008), had conducted a combined numerical and experimental analysis on Ahmed body with inclined

slant angles of 25° and 35°. Their findings showed that 3-D Ahmed body with 35° slant angle exhibited the better wake flow behind the rear portion, while in the case of Ahmed model with 25° of rear slope angle, the transition wake did not replicate the flow similar to experimental results. Howell et al. (2015) conducted a numerical study of aerodynamic behavior on different types of car body at various yaw angles. The results led to the conclusion that the change in vehicle yaw angle had significant impact on both side force and lift force of the vehicle which are the controlling factors for determining the stability of the vehicle. Howell et al. (2013). had researched on the simplified car body with different rear taper angle and taper length, their findings showed that drag reduction occurring at moderate taper angles and unfortunately drag is kept on increasing with increase in taper length. Koitrand et al. (2014). had proposed the aerodynamic models with moving front and rear wheels providing more precise data than the rigid ground method but it was a little bit cumbersome.

Littlewood et al. (2012). had conducted an experimental study on typical quarter scaled square back car model for drag reduction by the application of steady blowing jet technique with four configurations as an add-on device without re-profiling the outer surface. Their findings revealed that among four only one configuration showed expected peak drag reduction being attained at the event of maximum momentum coefficient. Marklund et al. (2013) performed a numerical study on sedan and wagon car models for the minimization of aerodynamic drag force and its consequent effects by incorporating under body cover and rear end diffusers into their vehicle models. The peak drag reduction rate was observed to be 8% and 5% for the sedan and wagon car models equipped with under body cover and rear diffuser respectively corresponding to the vehicle models having no under body cover and diffuser at its rear end. Selvaraju et al. (2016). had carried out a numerical prediction and experimental aerodynamic analysis on a typical car model for the estimation of drag force and pressure distribution characteristics in the mid plane of the car model using realizable (k- ε) model and 64 channel pressure scanner. The authors concluded that the obtained drag coefficient by means of computational and experimental methods were in close agreement with each other and that boundary layer thickness had greater impact in designing the vortex generator as an aerodynamic add-on device. Sadettin Hamut et al. (2014). had carried out the a numerical as well as experimental analysis of a typical race car model mounted with and without spoiler at the rear end, and got drag coefficient of 0.36 and 0.31 respectively and the lift value had been greatly reduced from 0.23 to 0.05 for the model having spoiler which would ensure stability of the vehicle. Tounsi et al. (2016) investigated the aerodynamic characteristics of Ahmed body having rear slant angle of 25° equipped with piezo-electric actuators at its top of rear window. The authors concluded that the reduced flow separation phenomenon and the development of
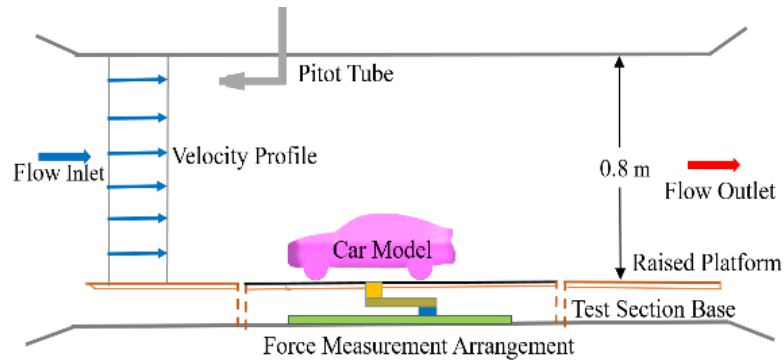
Fig. 1a. Layout of wind tunnel set-up.

small swirling motion of air had been observed when piezo-electric actuators were triggered on Wood *et al.* (2015). had carried out an experimental analysis on quarter scaled typical SUV car model in the wind tunnel by modifying its ride height and under floor roughness. The authors concluded that base pressure was mainly influenced by vehicle ride height, whereas variation in under floor roughness had only a minimal impact on the aerodynamic characteristics of the vehicle.

At present, very few research works have been carried out on semi active and actively operated air flow modifiers in the passenger car segment. An advanced type of semi actively controlled yaw angle of three delta shaped VGs that could minimize the aerodynamic forces by providing enhanced air flow guidance on the exterior profile of the car model that needed to be developed. As a novelty approach the VG yaw angles were modified by sending electrical pulse to the stepper motor, thereby the different yaw angle configurations of VGs could can be obtained and its corresponding aerodynamic forces were also quantified without interrupting the tunnel operation for adjusting the angular position of VG. In the previous literature only the flow characteristics of VG in fixed yaw angle alone has been studied by several researchers. In spite of reducing the complications in studying various aerodynamic aspects of VGs at different angles this system will provide platform for easier control of VG angles and also one can control the VG positions actively with respect to wind velocity by writing separate code for controlling the stepper controller for efficient operation of vehicles in different modes. The placement of VGs in optimal location of the vehicle body is the key element in determining the reduction of aerodynamic forces and its effects. In general, the VGs are positioned likely before the point of flow separation originating from the external surface of the vehicle body. Two stepper motors are employed to alter the yaw angle of two outer VGs, whereas VG in mid position remains unchanged throughout the analysis. The drag and lift reduction characteristics of these triple VGs in four dissimilar configurations are assessed quantitatively based on both experimenting in wind tunnel and computational fluid dynamics analysis on the simplified CAD car model.

2. EXPERIMENTAL INSTRUMENTS AND METHOD

2.1 Sub-Sonic wind Tunnel, Drag and Lift Coefficient Evaluation

A sub-sonic low-speed open circuit aerodynamic wind tunnel with a maximum wind speed capacity of about 55m/s has been used to evaluate the aerodynamic performance of physical car model equipped with semi actively controlled triple delta shaped VGs as an aerodynamic add-on device. The wind tunnel has test section dimensions of 2.0 m long, 0.8 m wide and 0.9 m high with a contraction ratio of 9:1. The schematic representation of the experimental setup is shown in Fig. 1a. The wind speed inside the test section is monitored with the help of inclined manometer connected to the pitot probe located on under side roof of the wind tunnel test section. The horizontal distance between inlet duct of the wind tunnel test section and front end of the car is 0.65m. The pitot probe is fixed at a height of 0.55m above the head of car and a linear horizontal distance of 0.25m from the front end of the car model. The turbulent intensity and flow uniformity of wind tunnel are not greater than 0.25% and 0.2% respectively. The aerodynamic drag and lift force acting on the testing model with respect to the appropriate wind velocity is quantified by means of dual cantilever type load cell set-up connected with the two separate digital force indicators. The sensitivity and data sampling rate of the aerodynamic drag and lift force measuring system is about 0.01N and 15 Hz respectively. The entire measuring arrangement is kept under the raised floor technique with a height of 0.1 m from the base of the wind tunnel test section. The vehicle model is affixed on the measuring tip of the load cell set-up while the force measuring system is rigidly bolted to the floor of the wind tunnel test section.

The coefficient of drag and lift forces are evaluated by considering the following equations.

$$C_D = \frac{2F_D}{\rho \times A \times V^2} \tag{1}$$

$$C_L = \frac{2F_L}{\rho \times A \times V^2} \tag{2}$$

Where F_D and F_L denotes the aerodynamic drag and

287

lift forces measured in parallel and perpendicular to the direction of the free stream respectively using digital force indicators, ρ is the density of air, A is the projected frontal area of the testing model, C_D and C_L are the coefficient of drag and lift respectively and lastly V is the velocity of the wind flowing inside the wind tunnel. The values of C_D and C_L can be obtained by using the Eqs. (1) and (2) respectively. The vehicle rested at zero yaw angle condition alone is tested in this work. However, the aerodynamic performance on the vehicle at various yaw angle condition is also considered to be much more significant.

2.2. Vehicle Model

The typical sedan car model along with triple VGs in four yaw angle configurations is experimentally investigated in this work. The overall vehicle model dimensions are 0.411m long, 0.165m wide and 0.140m high. One of the essential factors for wind tunnel testing is the blockage ratio, i.e., It is the ratio between the projected frontal area of the test model and the cross sectional area of the inlet duct of the wind tunnel test section, which is calculated to be as 3.42%. The raised floor height is also taken into account for determining the blockage ratio in all the cases of the experiments. West and Apelt (1982) suggested that whenever the actual blockage ratio is calculated to be as less than 6% the blockage correction factor can be omitted while re-calculating the experimentally obtained aerodynamics forces and pressure coefficient of the vehicle model using wind tunnel.

Fig. 2a. Car model with three delta profiled VGs.

Fig. 2b. Boundary layer separation point.

The vehicle model is equipped with triple delta shaped vortex generators shown in Fig. 2a. The VGs are located on the roof end of the car model where the flow separation originates from its exterior profile. The boundary layer separation region has been observed by passing the dense fumes over the

base model using smoke generator as shown in Fig. 2b. The existence of separated flow from the vehicle is observed in the rear end roof portion of the car body. Hence with the VGs being fixed in the particular position the entire analysis was carried out. The outer two VGs placed on either side were coupled to the armature of the mini stepper motor which was mounted on the underside roof of the car model. The key benefits of this set-up is to reduce the experiment time because the VGs yaw angles can be controlled easily even in the wind tunnel operating condition. So there is no need to interrupt the experiment by stopping the wind tunnel and modify the VGs Yaw angle manually for each and every case, thereby reducing the complexity and time duration to conduct the experiments.

3. DESIGN OF VORTEX GENERATORS AND SELECTION OF OPTIMAL VG DESIGN

A traditional and benchmark aerodynamic road vehicle reference model called Ahmed body shown in Fig. 3a. has been utilized to quantify the best VG design among the four different cross sections of VGs named as D1, D2, D3, and D4 respectively. Ahmed body with the position of three VGs of design D3 is displayed in the Fig. 3b. Initially CAD geometry of half scaled down Ahmed body having a length of 0.511m, width of 0.195m and height of 0.144m was generated using typical CAD modelling software.
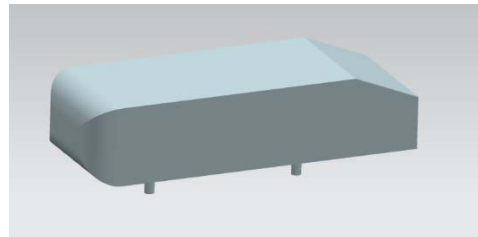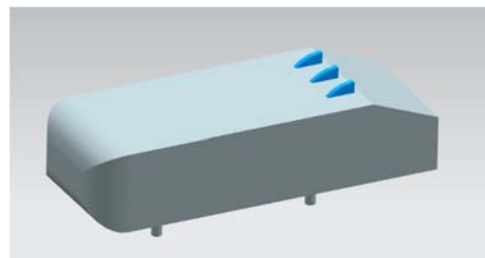

Fig. 3a. Base Ahmed model.

Fig. 3b. Ahmed body with three D3 design of VGs.

Ahmed body was bounded with the computational domain of 9L long, 4L wide and 3L high where L denotes the length of the Ahmed model. The computational domain around the Ahmed model has been discretized using prism layered mesh with grid height of 0.9 mm, height ratio of 1.1 and 4.2×10^6 number of elements approximately used as standard grid parameters for all the cases of numerical

simulation. The Ahmed body without VGs has been analysed computationally using realizable (k- ε) model considering the inlet velocity of air being about 50m/s. The coefficients of drag and lift force for the Ahmed body without VGs were found to be 0.285 and 0.323 respectively.

The design of vortex generators is mainly based on the thickness of boundary layer observed in flow separation point of the vehicle body. The nomenclature of delta shaped VG is shown in Fig**.** 3c. The interior angles of the delta profiled VG a, b, and c were 36°, 86° and 58° respectively. The boundary layer thickness was measured to be 20mm approximately which was at the rear end roof portion of the Ahmed body. Masaru koike et.al recommended that height of VG should be equivalent to thickness of boundary layer, length to be two times the height of VG and lastly width or thickness of VG to be equivalent to one-fourth of the height of VG. Hence all the four different shapes of VG were designed based on the above relation and the same design procedure was followed in designing of VG for the car model.

Later the Ahmed body mounted with three numbers of individual design of VGs were numerically simulated with four dissimilar designs of three VGs on its roof and it was seen that Ahmed body having D4 and D2 VG design exhibited the least drag and lift coefficients of 0.278 and 0.315 respectively.
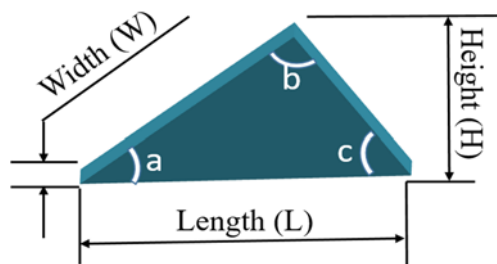

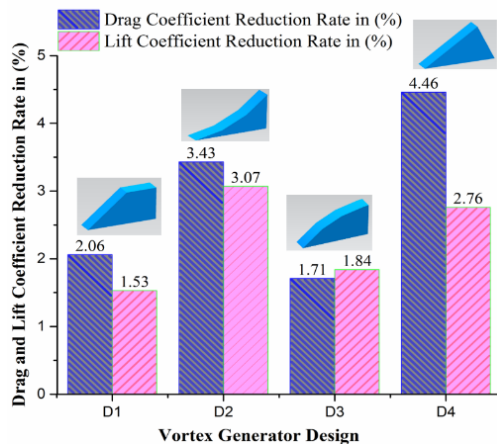**Fig. 3c. Delta shaped vortex generator (VG) nomenclature.**

Fig. 3d. Drag and lift reduction rate of Ahmed body with four different VG design.

The results of coefficients of drag and lift force reduction rate for the four dissimilar VG design are presented in the Fig. 3(i). It is evident that the Ahmed body with D4 and D2 design unveils the highest drag and lift coefficient reduction rate of 4.46% and 3.07% relative to the standard Ahmed model. In lieu of selection of optimal VG design, more weight is given to the reduction of coefficient of drag than lift and hence D4 design was considered as an effective one for the typical car model to reduce the effects of aerodynamic forces at all wind velocities.

4. VORTEX GENERATOR YAW ANGLE CONTROLLER CIRCUIT

The two stepper motors were used to modify the yaw angle of the outer two VGs. The stepper motors were precisely controlled by a separate electronic programmed circuit layout that is shown in Fig. 4a. It was powered by an Arduino Uno circuit board. The four different configurations of VGs were obtained using the electronic controlling circuit shown in Fig. 4b. The push button was provided in the VG yaw angle controlling unit to attain the stepper motor minimum step angle of 1.4° in a single press of the switch. This circuit was designed to operate the stepper motors in both clock wise and anti-clock wise directions so that the experimental complications could be reduced.
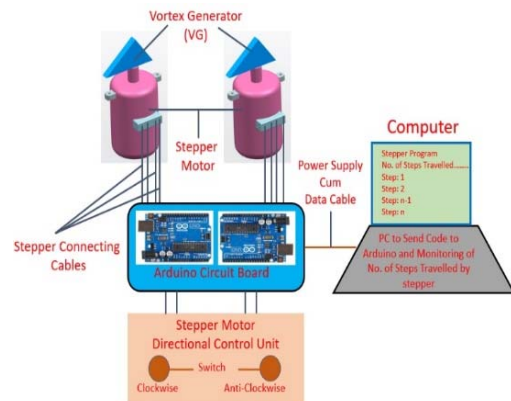

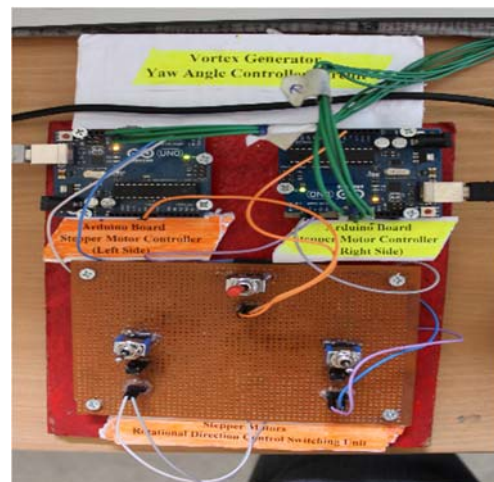**Fig. 4a. Schematic layout of VG semi active control system.**

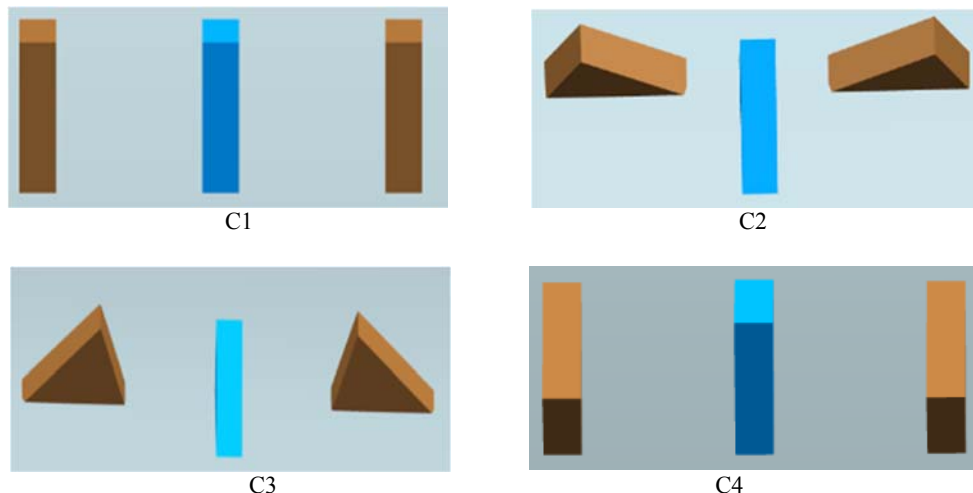**Fig. 4b. Electronic circuit to control stepper motor.**

Fig. 5a. Four different configuration of three VGs.

5. RESULTS AND DISCUSSIONS

The four dissimilar configurations of three delta profiled VGs are shown in the Fig. 5a. The car model without vortex generators exhibits similar drag coefficient over the entire range of wind velocities ranging from 10m/s to 50m/s with an increment velocity of 10m/s. But in the case of lift coefficient, the trend is similar to the inverted U curve as shown in Fig. 5b. for the same measured velocities.
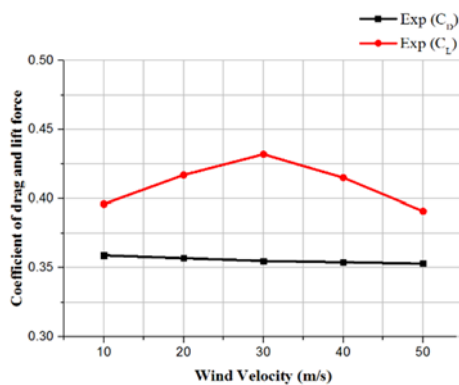

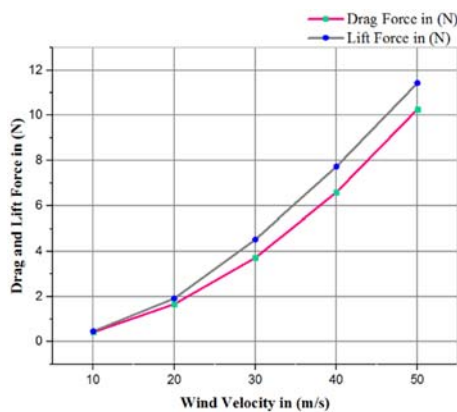**Fig. 5b. Coefficient of drag and lift variation.**

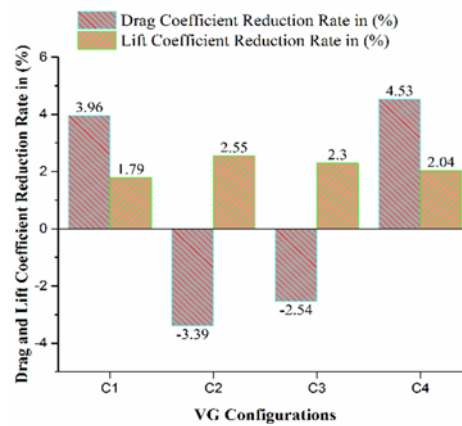**Fig. 5c. Drag and lift force variation.**

Fig. 5d. Coefficients of drag and lift force reduction rate for four different VG configurations.

The boundary layer thickness for car model was measured to be as 25mm and VG for vehicle model was designed based on the design procedure of VG for Ahmed model which has been discussed earlier. The drag and lift coefficients of the base car model at wind speed V_{wind} = 50m/s were got to be 0.353 and 0.391 respectively. The drag and lift force for the same wind speeds is presented in the Fig. 5c. By using Eq. (3) the Reynolds number for this case was obtained to be as 1.423×10^6 based on the length

$$R_e = \frac{\rho_{air} \times V_{Wind} \times \ell}{\mu} \qquad (3)$$

of the car model (0.411m), Where ρ_{air} is the density of air, V_{Wind} is wind velocity, μ is kinematic viscosity of air and ℓ is the length of the car model. Among the four different cases the effects of drag reduction were highly distinctive when the outer VGs were facing towards the rear part of the vehicle (i.e.) in the case of C4 configuration. The coefficients of drag and lift force reduction rate for all the four configurations of VG relative to the base line model are displayed in the Fig. 5d. From the results with C2 and C3 configurations, the magnitudes of drag

coefficient exceed (indicated with negative sign) the base line model drag coefficient by -2.54% and -3.39% respectively. The above instance is mainly due to the deflection of air in the upward direction causing an increased wake region behind the car model leading to the formation of large pressure imbalance between the front and the rear portion of the vehicle body. But in contrast the lift force coefficient of C2 and C3 configurations unveils increased reduction rate than the other two cases relative to the standard car model.

The VGs positioned in perpendicular to the wind direction result in diverting the air in an upward motion causing increase in negative lift characteristics of the vehicle which improves the traction and tractive effort of the vehicle. The model with C1 and C4 configurations evinces better drag coefficient reduction characteristics than the model with C2 and C3 pattern of VGs. In the cases of vehicle model with VGs in C1 and C4 configurations the VGs are positioned in such a way that they are parallel to the wind flow direction thus they have better properties in minimizing the flow separation from the vehicle body. This reduces the global pressure difference between the front and the aft portions of the car model, which has a notable positive impact on increasing the fuel efficiency of the vehicle. It has been concluded that the car model having the VGs in C4 and C2 configuration provides the maximum drag and lift coefficient reduction rates of 4.53% and 2.55% respectively compared with the reference model.

6. COMPUTATIONAL FLUID DYNAMICS SIMULATION

6.1 Computational Analysis Methodology and Its Results

The computational simulation using simplified CAD geometry is shown in Fig. 6a, identical to the external dimensions of the physical car body being performed using realizable (k- ε) as a simulation code which can highlight the unsteady flow pattern around the vehicle model with sufficient detail. Singh *et al.* (2005). carried out a computational analysis on a truck model to examine the effects of boundary layer separation and made a comparative study between the four different solver models in CFD ANSYS – GAMBIT, namely (Standard k-ε, Spalart-Allmaras, Renormalization group k- ε, and Realizable k-ε). It has been concluded that realizable k- ε method provides better results when compared with the other three methods. There are two advanced numerical simulation models called large eddy simulation (LES) and detached eddy simulation (DES) techniques are available in most of the CFD codes which can reveal the flow pattern around the bodies in an excellent manner but both the model requires high configuration computers that cause increase in the computation cost. The large eddy simulation LES models can predict the flow where the formation of large turbulent eddies occurs around the system but they will provide less information about the turbulent scales near the walls of the system. The detached eddy simulation DES technique is the hybrid of the

RANS and LES method which can resolve the demerits of LES technique and provide detailed turbulent information in the region near the walls of the system. The singular values sub-grid model (SIGMA) is the typical sub-grid model which was derived from the analysis of singular values of resolved velocity gradient tensor and it uses the invariants of spatial filtered strain tensor to model the eddy viscosity around the walls of the system. The SIGMA model offers lesser computation cost and it reduces the complexity in performing the computation of non-homogenous wall-bounded flows. The computational domain was created to enclose the car geometry with its overall dimensional details being 9L, 4L, and 3L corresponding to the longitudinal axis, lateral axis and vertical axis respectively of the car model. All the dimensions of the domain are made relative to the length of the car model (L). The upstream and the downstream distances of fluid domain were set to be 2L and 6L respectively. No slip boundary condition was applied to all the surfaces of computation domain and wall boundaries of the vehicle model. Uniform flow at the inlet zone of the domain was attained by applying the condition as zero boundary layer thickness and the turbulence intensity of 0.25%. Computational flow configuration with coordinate axis of the vehicle model is shown in Fig. 6b. Moreover, the numerical flow physics is kept closer to the
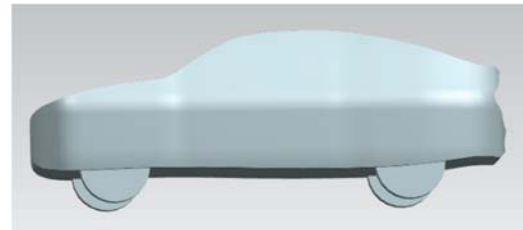

Fig. 6a. CAD model of simplified car geometry.

ambiance of the experimental analysis. The inlet velocity of air was given as 50m/s relative to the experimental Reynolds number of the car model. The grid independence test was carried out prior to the numerical simulation because the number of cells in the fluid domain has considerable impact in affecting the solutions of CFD analysis.
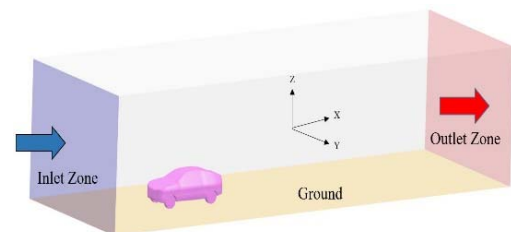

Fig. 6b. Different regions of computational domain.

The results of grid independence test are illustrated in Table. 1. The entire fluid domain was discretized with prism layered mesh composed of 3.8×10^6 number of elements approximately and considering

Table 1 Grid independence test results

Total number of elements (1×10^6)	First wall distance in (mm)	Grid spacing ratio	Coefficient of drag (C_D)	Coefficient of lift (C_L)	Computation duration in (Hours)
2.8	1.5	2.5	0.361	0.399	6
3.2	1.2	1.6	0.358	0.395	8
3.8	0.8	1.2	0.353	0.391	10
4.2	0.6	1.1	0.351	0.389	13

Table 2 Boundary conditions at various regions of fluid domain

Computational Regimes	Applied Boundary Conditions
Inlet	Velocity Inlet
Outlet	Pressure Outlet (Reference Pressure 0 pa)
Top, Sides and Ceiling	No-Slip wall Condition
Ground	Fixed ground with No-Slip wall Condition

Table 3 Numerical drag and lift coefficient reduction rate for four configurations of VG

Case Number	Coefficient of drag (C_D)	Coefficient of lift (C_L)	Reduction rate of drag coefficient in (%)	Reduction rate of lift coefficient in (%)
Base	0.347	0.388	-----	-----
C1	0.336	0.382	3.74	1.54
C2	0.355	0.379	-2.30	2.31
C3	0.358	0.380	-3.17	2.06
C4	0.332	0.381	4.32	1.80

the initial grid layer height and grid height ratio of 0.8mm and 1.2 respectively as the standard level of grid for all the cases.
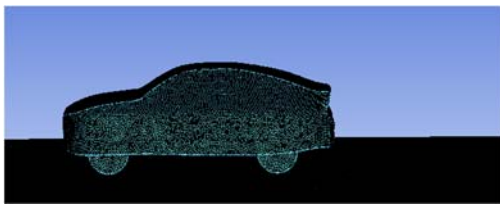

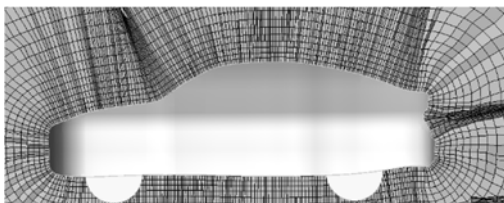**Fig. 6c. Overall view of numerical grid around the model.**

Fig. 6d. Computational grid at mid plane of car model.

The computational cells were generated by using local refinement method and the images of numerical grid around the simplified car geometry are shown in Fig. 6c. The boundary conditions at different regimes of the computational domain are given in Table. 2.

The formation of grid at the entire car model and central plane with respect to the lateral axis of the vehicle is shown in Fig. 6d. The realizable (k- ε) method with SIMPLE (Semi-Implicit Pressure Linked Equation) algorithm was used as an iterative scheme and considering spatial discretization gradient as least squares cell based method. The pressure, momentum, turbulent kinetic energy and turbulent dissipation rate were set to follow the second order upwind scheme for iterating the numerical simulation. The numerically estimated values of aerodynamic drag and lift coefficients for base car model using realizable (k- ε) method were 0.347 and 0.388 respectively. The aerodynamic drag and lift coefficients for vehicle model without and with VG for four yaw angle configurations obtained from numerical analysis are illustrated in the Table. 3.

The numerically predicted drag and lift coefficients of the car model without and with VGs are slightly under the estimates of the experimental results. However, the coefficient of drag and lift force for the

Table 4 Deviation of results between wind tunnel and computational methods.

Configuration	Error analysis between experimental and numerical results in %	
	Coefficient of drag (C_D)	Coefficient of lift (C_L)
Base	2.5	2.4
C1	2.7	3.1
C2	2.9	2.2
C3	3.2	2.6
C4	2.8	2.3

car model obtained from the results of wind tunnel and computational methods were closely correlating with each other by showing maximum deviation of about 3.2%.

Hence it is evident that the numerical model predicted the aerodynamic coefficients closer to the results of experimental analysis. The existence of result deviation between the empirical and numerical simulation methods is presented in Table. 4. The profile drag is the predominant factor in deciding the existence of pressure difference between the fore and the aft portions of the vehicle model, whereas skin friction plays only a minimal role in determining the magnitude of aerodynamic forces acting on the vehicle with respect to its moving velocity. In the present work, the intensity of form drag has been trimmed by incorporating the triple delta shaped VGs located on the tail end roof of the car model to minimize the low pressure region behind the vehicle body. Based on the results of computational analysis, it can be stated that the model with C4 and C2 configuration exhibits the peak reduction rate of 4.32% in drag force coefficient and 2.31% in lift coefficient compared with the standard model.

6.2 Flow Pattern

The velocity gradient around the symmetrical plane of the reference car model is shown in the Fig. 7 which can reveal the velocity magnitude at all the boundaries of the car model. The magnitude of turbulent kinetic energy for the reference model in its roof section is shown in Fig. 8a. it unveils the formation of higher turbulent kinetic energy gradient in the aft portion of the car body. Likewise, the car model with C2 and C3 configurations is shown in Fig. 8c. and Fig. 8d. It exhibits the similar trend of turbulent kinetic gradient at its rear portion when compared with the turbulent kinetic energy contour of the reference model. The existence of above instance is mainly due to the placement of VGs in perpendicular position to the wind direction causing larger flow separation from the vehicle body post to the region of VGs. The rise in turbulent kinetic energy gradient causes increased pressure imbalance between anterior and posterior portions of the car body which affects the performance of the vehicle to a great extent and also it trims the fuel economy.
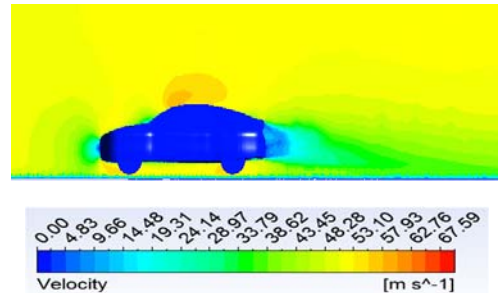

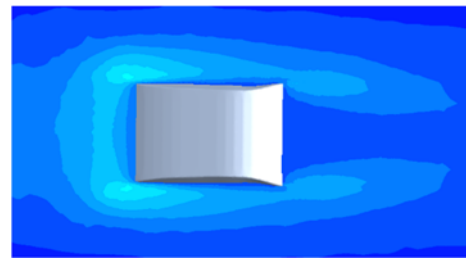**Fig. 7. Velocity gradient around the Base model.**

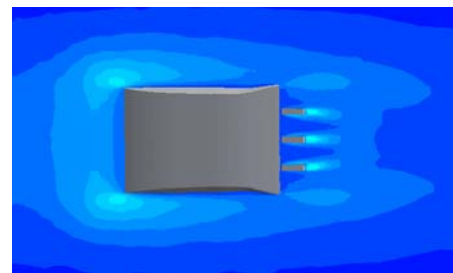**Fig. 8a. Turbulent-kinetic energy for Base model.**

Fig. 8b. Turbulent-kinetic energy for car model with C1 configuration.
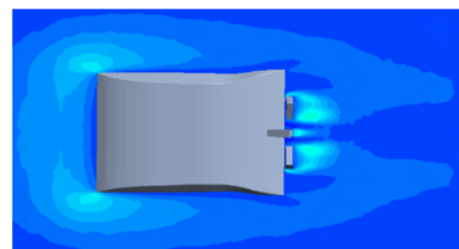

Fig. 8c. Turbulent-kinetic energy for car model with C2 configuration.
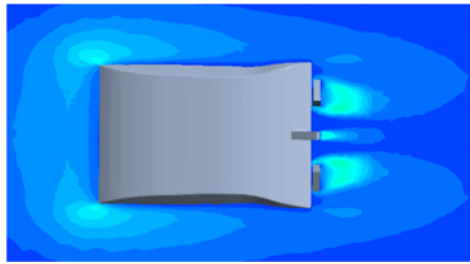
Fig. 8d. Turbulent-kinetic energy for car model with C3 configuration.
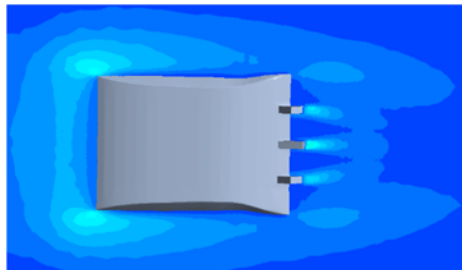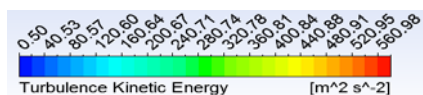

Fig. 8e. Turbulent-kinetic energy for car model with C4 configuration.

In contrast to the phenomenon of turbulent kinetic energy distribution, the vehicle having C1 and C4 configurations evinces the attenuated trend of turbulent energy variation as shown in Fig. 8b. and Fig. 8e. past to the vehicle model. The VGs are positioned in such a way as to enhance the flow attachment with the vehicle body and provide a minimal pressure difference between the anterior and the posterior portions of the car body.

Even though the cases C1 and C4 explore very little variation in showing the attenuated trend of turbulent kinetic energy gradient at the roof plane of the car model, the C4 design exhibits superior performance in showing the attenuated form of kinetic energy behind the VGs than that of the reference model including the other three cases of VGs. As a result, the reduced effects of aerodynamic forces and considerable improvement in fuel economy characteristics of the vehicle can be attained when the VGs are positioned in C4 configuration.

7. CONCLUSION

This paper has reported on an extensive study of aerodynamic drag and lift coefficients and their effects on typical sedan car model mounted with four different yaw angle configurations of three delta shaped VGs that were quantitatively determined by experimental and computational analysis. The car model with VGs in C1 and C4 configurations has exhibited a similar trend in the reduction of drag coefficient, while the vehicle model with VGs in C2 and C3 pattern has unveiled a reduced tendency of lift coefficient compared with the car model without VGs. A comparison of all the four cases has revealed the maximum drag and lift coefficient reduction rate of 4.53% and 2.55% is observed for the cases of car model having VGs in C4 and C2 configurations respectively related to the standard car model.

Even though the vehicle with VGs in C2 configuration exhibits greater drag coefficient than the remaining cases resulting in restricting the forward motion of the vehicle, the same opposing drag force can be converted in to other forms of useful work in the instance of braking (Decelerating) the vehicle from higher velocities, by programming the control system of the stepper motor to position the VGs in C2 pattern at the time of braking alone. Hence the increased drag force is having the ability to decelerate the vehicle by providing additional aerodynamic resistance along with the mechanical frictional resistance generated by the braking system of the vehicle. When the vehicle brake is released, the VGs are allowed to reposition to C4 configuration using the same VGs yaw angle controlling system in order to improve the aerodynamic performance of the vehicle even at its increased speeds.

The realizable (k- ε) model estimates the coefficient of aerodynamic drag and lift force closer to the experimental testing results. The vehicle model with C2 configuration of VGs has the peak negative lift coefficient compared with the reference model. The increment in the negative lift coefficient improves the vehicle stability and its handling characteristics by providing an increased downward force on the vehicle body.

The car model with C4 configuration has exhibited attenuated turbulent kinetic energy distribution between the anterior and the posterior portions of the vehicle body rather than the other three remaining cases. The lift coefficient reduction rate of C4 case is closer to the values of C2 and C3 configurations of VGs. From this research it is concluded that the position of VGs in C4 pattern exposes the enhanced properties in minimizing the phenomenon of air flow detachment from the exterior profile of the vehicle model which results in increased stability by providing least resistance to the forward motion of the vehicle relative to the model without vortex generators.

REFERENCES

Aider, J. L., J. F. Beaudoin and J. E. Wesfreid (2010). Drag and lift reduction of a 3D bluff-body using active vortex generators. *Experiments in fluids 48*(5), 771-789.

Aljure, D. E., O. Lehmkuhl, I. Rodriguez and A.

Oliva (2014). Flow and turbulent structures around simplified car models. *Computers and Fluids 96*, 122-135.

Bello Millán, F. J., T. Mäkelä, L. Parras, C. Del Pino and C. Ferrera (2016). Experimental study on Ahmed's body drag coefficient for different yaw angles. Journal of Wind Engineering and Industrial Aerodynamics 157, 140-144.

Birwa, S. K., N. Rathi and R. Gupta (2013). Aerodynamic analysis of Audi A4 Sedan using CFD. *Journal of The Institution of Engineers (India): Series C*, *94*(2), 105-111.

Castro, N., O. D. Lopez and L. Munoz (2013). Computational prediction of a vehicle aerodynamics using detached Eddy simulation. *SAE International Journal of Passenger Cars-Mechanical Systems 6*(2013-01-1254), 414-423.

Gillieron, P. and A. Kourta (2013). Aerodynamic drag control by pulsed jets on simplified car geometry. Experiments in fluids 54(2), 1-16.

Gopal, P. and T. Senthilkumar (2013). Influence of Wake Characteristics of a Representative Car Model by Delaying Boundary Layer Separation. *Journal of Applied Science and Engineering* 16(4), 363-374.

Guilmineau, E. (2008). Computational study of flow around a simplified car body. *Journal of wind engineering and industrial aerodynamics 96*(6), 1207-1217.

Howell, J. (2015). Aerodynamic Drag of Passenger Cars at Yaw, *SAE SAE International of journal of Passenger Cars - Mech. Syst.* 8(1), 306-316.

Howell, J., M. A. Passmore and S. Tuplin (2013). Aerodynamic drag reduction on a simple car-like shape with rear upper body taper. SAE Internation journal for passenger cars-Mech syst 6, 52-60.

Koike, M., T. Nagayoshi and N. Hamamoto (2004). Research on aerodynamic drag reduction by vortex generators. *Mitsubishi motors technical review16*, 11-16.

Koitrand, S., L. Lofdahl, S. Rehnberg and Gaylard,

A., (2014). A Computational Investigation of Ground Simulation for a Saloon Car. *SAE International Journal of Commercial Vehicles 7*(2014-01-0615), 111-123.

Littlewood, R. P. and M. A. Passmore (2012). Aerodynamic drag reduction of a simplified square back vehicle using steady blowing. *Experiments in fluids 53*(2), 519-529.

Marklund, J., L. Lofdahl, H. Danielsson and G. Olsson (2013). Performance of an Automotive Under-Body Diffuser Applied to a Sedan and a Wagon Vehicle," *SAE International of journal of Passenger Cars - Mech. Syst.* 6(1), 293-307.

Sadettin Hamut, H., R. Salah El Emam, M. Aydin and I. Dincer (2014). Effects of rear spoilers on ground vehicle aerodynamic drag. *International Journal of Numerical Methods for Heat and Fluid Flow 24*(3), 627-642.

Selvaraju, P. N. and K. M. Parammasivam (2016). Numerical and experimental investigations of drag force on scaled car model. *thermal science* 20(4), 1153-1158.

Singh, S. N., L. Rai, P. Puri and A. Bhatnagar (2005). Effect of moving surface on the aerodynamic *Institution of Mechanical Engineers, Part D: Journal of Automobile Engineering 219*(2), 127-134.

Tounsi, N., R. Mestiri, L. Keirsbulck, H. Oualli, S. Hanchi and F. Aloui (2016). Experimental study of flow control on bluff body using piezoelectric actuators. *Journal of Applied Fluid Mechanics* 9(2), 827-838.

West, G. S. and C. J. Apelt (1982). The effects of tunnel blockage and aspect ratio on the mean flow past a circular cylinder with Reynolds numbers. *Journal of Fluid mechanics*, 114, 361–377.

Wood, A., M. Passmore, D. Forbes, D. Wood and A. Gaylard (2015). Base Pressure and Flow-Field Measurements on a Generic SUV Model. *SAE International Journal of Passenger Cars-Mechanical Systems*, *8*(2015-01-1546), 233-241.